Time Efficient Ultrasound Localization Microscopy

Zhehao Shen
ShanghaiTech University
Shanghai, China
shenzhh@shanghaitech.edu.cn

Hengan Zhou
ShanghaiTech University
Shanghai, China
zhouha@shanghaitech.edu.cn

Fuqiang Zhao
ShanghaiTech University
Shanghai, China
zhaofq@shanghaitech.edu.cn

I. Introduction

Ultrasound stands as a key medical imaging technique for visualizing subcutaneous body structures such as organs, muscles, and arteries due to its safety, affordability, and non-invasive nature. However, traditional ultrasound systems are limited by the diffraction limit, which restricts spatial resolution to the wavelength scale. Although higher frequencies can enhance spatial resolution, they reduce the beam's penetration depth, resulting in a trade-off between resolution and penetration depth.

In recent years, to address the trade-off between spatial resolution and penetration depth, an innovative method called Ultrasound Localization Microscopy (ULM) [6] has been developed. ULM effectively resolves this issue by individually localizing and tracking intravenously injected microbubbles (MBs), also known as ultrasound contrast agents (UCAs). When the microbubbles are sufficiently separated, the centroid of each MB can be pinpointed with an accuracy ten times finer than the wavelength. By aggregating the centroids of single echoes produced by these UCAs, ULM can surpass the traditional ultrasound diffraction limit. Ultimately, by tracking the microbubbles as they flow through the vascular system, ULM achieves super-resolution vascular imaging. These high-quality images are crucial for understanding and diagnosing vascular-related diseases such as cancer, stroke, and atherosclerosis. The ULM's pipeline is shown in Fig. 1.

Despite the potential advantages of Ultrasound Localization Microscopy (ULM) in clinical applications, its use is currently limited by two main practical challenges. First, low concentrations of microbubbles (MBs) and long acquisition times are required to record sufficiently separated MB echoes for accurate localization and tracking. Second, a high frame rate is necessary to consistently pair the MB signals from one frame to the next. These demands for long acquisition times and high frame rates have hindered the clinical translation of ULM. Specifically, ULM generates noticeable noise when processing low-frequency data inputs compared to high-frequency data inputs, as illustrated in Fig. 2.

There are several methods to address this issue. One approach is to directly increase the concentration of microbubbles (MBs), but this can result in overlapping MB signals, making it difficult to distinguish and individually localize different MB echoes. Ackerman [1] implemented a modified Markov chain Monte Carlo data association method to recover ultrasound contrast agent (UCA) tracks at lower frame rates, though this method often incurs significant computational costs. Other approaches [8], [11]leverage deep learning architectures to localize MBs in dense scenarios. However, deep learning requires a substantial amount of labeled data for model training and testing, which is challenging to obtain.

Therefore, following the approach outlined in the [10], we applied 2D spatial-temporal RBF interpolation in the original image sequences to achieve upsampling.

II. Methods

A. Framework

We adapt the pipeline proposed by [6], which consists of four basic steps: data pre-processing and filtering, MB detection, MB localization and tracking, and accumulation. We pre-process the data acquired at high frame rates with singular value decomposition (SVD) spatio-temporal filtering, which distinguishes the MBs signal from the surrounding tissue by reducing clutter and tissue noise [3].

Next, MB signals are detected based on the pixels intensity in each frame, where we select the top n pixels in each frame by intense values. Individual MBs are then localized by fitting to a 2D multivariate Gaussian distribution with uniform standard variation along both axis.

The tracking algorithm is a modification of the Khun-Munkres bipartite tracking algorithm, as in [7]. Due to uncertainties in estimating the number of MBs per frame during localization, sub-optimal solutions can result. Additionally, unpredictable UCAs events like MB appearance/disappearance may also cause sub-optimal outcomes. Thus, the Khun-Munkres algorithm is modified for partial assignment: an MB in frame f that exhausts all assignment options in frame $f+1$ is discarded [9]. Additionally, a threshold on the minimum length of a track is applied to further strengthen the robustness of the tracking performance [10].

Finally, an SR intensity map is obtained by accumulating the tracks, previously smoothed and interpolated to fill in the missing points, over all frames.

B. RBF Interpolation

Following the pipeline of [10], shown in Fig. 3, we start by unfolding an $H \cdot W \cdot T$ image sequence along the W dimension, resulting in W images of size $H \cdot T$. We then use the pixel indices in the $H \cdot T$ images as the variable X in 2D.

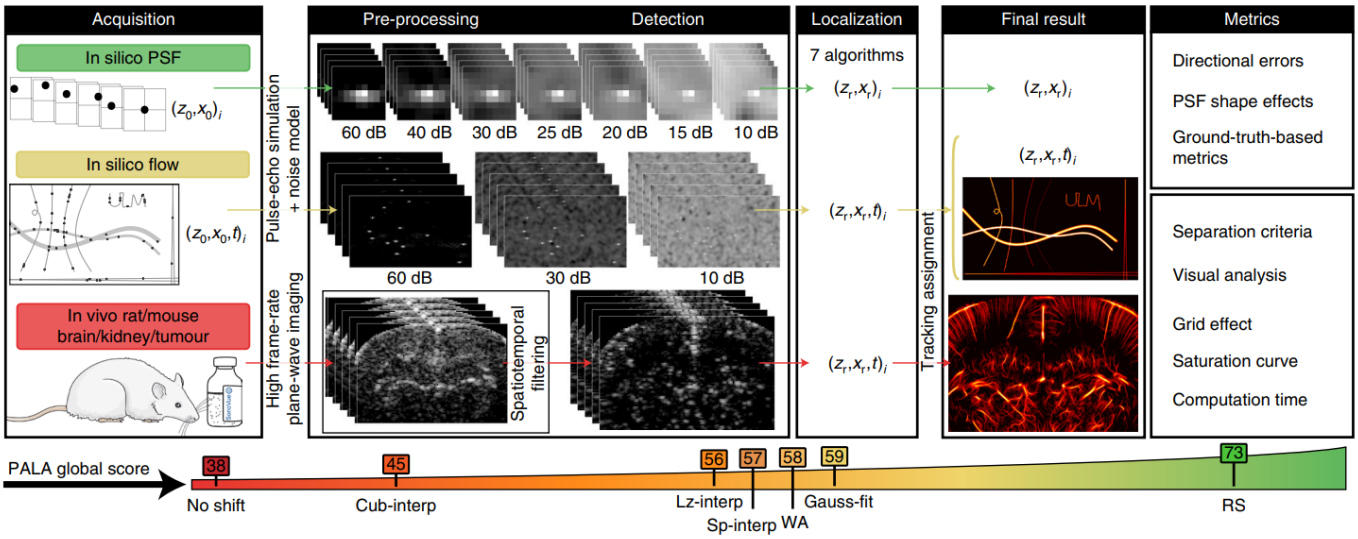

Fig. 1. The pipeline of ULM.

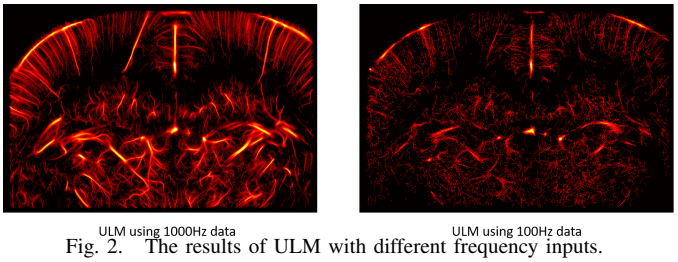

Fig. 2. The results of ULM with different frequency inputs.

Using the distance function $r_{i,j}$ and the kernel function $\phi(r)$,

$$r_{i,j} = ||I_i - I_j||_2^2 \tag{1}$$

I_i is (x,y) index of i pixel in H-T image

$$\text{GA kernel: } \phi(r) = e^{-\epsilon \cdot r^2} \tag{2}$$

$$\text{IMQ kernel: } \phi(r) = \frac{1}{\sqrt{1 + (\epsilon \cdot r)^2}} \tag{3}$$

The RBF matrix

$$\begin{bmatrix} \phi(r_{1,1}) & \phi(r_{1,2}) & \dots & \phi(r_{1,N}) \\ \phi(r_{2,1}) & \phi(r_{2,2}) & \dots & \phi(r_{2,N}) \\ \dots & \dots & \vdots & \vdots \\ \phi(r_{N-1,1}) & \phi(r_{N-1,2}) & \dots & \phi(r_{N-1,N}) \\ \phi(r_{N,1}) & \phi(r_{N;2}) & \dots & \phi(r_{N,N}) \end{bmatrix}$$

are constructed by the kernel and distance function. By solving a linear system of equations:

$$\phi(r,\tau) \cdot \begin{bmatrix} \beta_1 \\ \beta_2 \\ \dots \\ \beta_{N-1} \\ \beta_N \end{bmatrix} = \begin{bmatrix} f(\mathbf{X}_1) \\ f(\mathbf{X}_2) \\ \dots \\ f(\mathbf{X}_{N-1}) \\ f(\mathbf{X}_N) \end{bmatrix}$$

, τ is a shape parameter which is a hyper-parameter, we obtain the RBF node functions for interpolation. Based on the original data's downsampling rates (2x, 4x, 10x), we then upsample and construct $H \cdot 2T$, $H \cdot 4T$, and $H \cdot 10T$ as H, which serve as the variable values for interpolation. Finally, we perform the interpolation by solving another linear system of equations and we can get the result by the equation below:

$$\mathbf{F}_{est} = \mathbf{HB} = \mathbf{H\Phi}^{-1}\mathbf{F}$$

C. Hyper-parameter Tuning

However, the interpolation method described above has a significant issue. Although the Gaussian kernel and IMQ kernel used to construct the ϕ function ensure non-negativity and the positive definiteness of the matrix, we discovered during implementation that the matrix has an extremely large condition number. This makes solving the linear system an ill-posed problem, resulting in substantial numerical computation errors. Therefore, based on the Hardy [5] and the Frank [4] approaches, we adjusted our shape parameter to limit the condition number of the ϕ matrix.

III. Results

TABLE I
RMSE BETWEEN DIFFERENT METHODS AND KERNEL FUNCTIONS

Methods	RBFs	DS rates		
		2	4	10
ULM	-	4.50	4.46	4.52
TEULM	GA	**4.22**	4.30	4.64
TEULM	IMQ	4.23	4.31	4.64

TABLE II
DICE SCORE BETWEEN DIFFERENT METHODS AND KERNEL FUNCTIONS

Methods	RBFs	DS rates		
		2	4	10
ULM	-	0.815	0.711	0.398
TEULM	GA	**0.900**	0.819	0.787
TEULM	IMQ	0.886	0.793	0.788

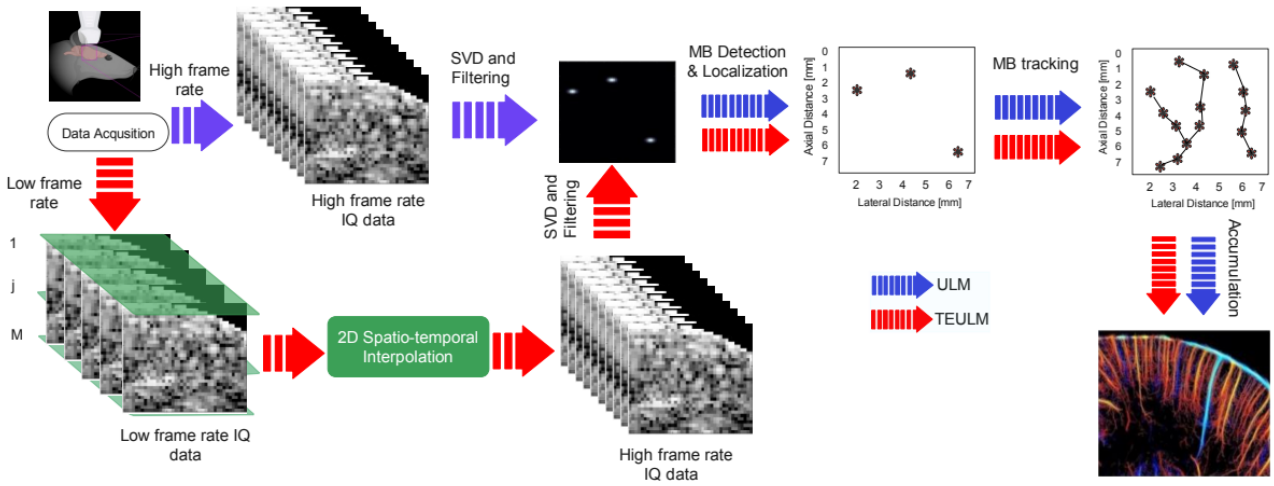

Fig. 3. The pipeline of TEULM.

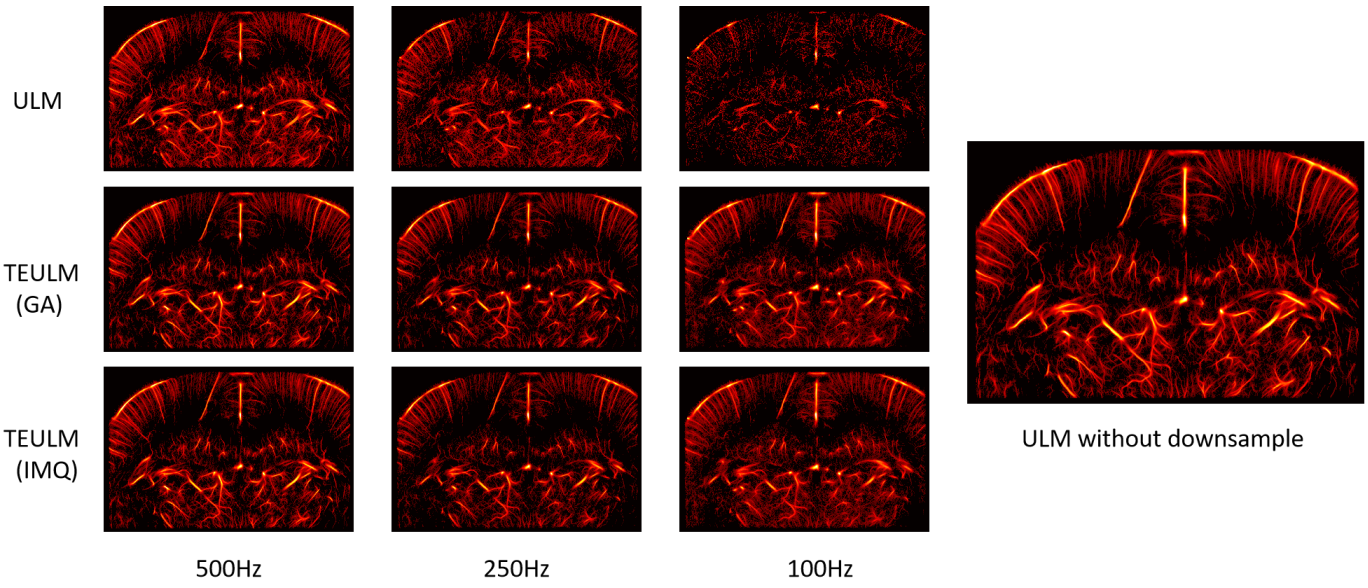

Fig. 4. The Visualization results of TEULM and comparison to ULM.

We used RMSE and Dice Score to evaluate the effectiveness of our method. The definitions of RMSE and Dice Score are as follows:

$$RMSE = \sqrt{\frac{1}{N}\sum_{i=1}^{N}(x_i - \hat{x}_i)^2} \tag{4}$$

$$Dice = \frac{2|A \cap B|}{|A| + |B|} \tag{5}$$

The numerical results for RMSE and Dice Score for different RBF functions and methods are presented in Tab. I and Tab. II From the tables, we observe that the TEULM algorithm significantly outperforms the original ULM method. Additionally, in terms of kernel function selection, we find that the Gaussian kernel outperforms the IMQ kernel. Based on our analysis, this is likely due to the exponential decay characteristic of the Gaussian kernel, which tends to provide smoother interpolation. This results in more accurate and stable interpolation, especially in areas with high-frequency variations. Furthermore, our review of mathematical literature [2] indicates that, compared to the IMQ kernel, the Gaussian kernel typically has a lower condition number, leading to more reliable numerical solutions.

REFERENCES

[1] Dimitri Ackermann and Georg Schmitz. Detection and tracking of multiple microbubbles in ultrasound b-mode images. *IEEE transactions on ultrasonics, ferroelectrics, and frequency control*, 63(1):72–82, 2015.

[2] Martin Dietrich Buhmann. Radial basis functions. *Acta numerica*, 9:1–38, 2000.

[3] Charlie Demené, Thomas Deffieux, Mathieu Pernot, Bruno-Félix Osmanski, Valérie Biran, Jean-Luc Gennisson, Lim-Anna Sieu, Antoine Bergel, Stéphanie Franqui, Jean-Michel Correas, Ivan Cohen, Olivier Baud, and Mickael Tanter. Spatiotemporal clutter filtering of ultrafast ultrasound data highly increases doppler and fultrasound sensitivity. *IEEE Transactions on Medical Imaging*, 34(11):2271–2285, 2015.

[4] Richard Franke. Scattered data interpolation: tests of some methods. *Mathematics of Computation*, 38:181–200, 1982.

[5] Rolland Lee Hardy. Multiquadric equations of topography and other irregular surfaces. *Journal of Geophysical Research*, 76:1905–1915, 1971.

[6] Baptiste Heiles, Arthur Chavignon, Vincent Hingot, Pauline Lopez, Eliott Teston, and Olivier Couture. Performance benchmarking of microbubble-localization algorithms for ultrasound localization microscopy. *Nature Biomedical Engineering*, 6(5):605–616, 2022.

[7] Harold W. Kuhn. *The Hungarian Method for the Assignment Problem*, pages 29–47. Springer Berlin Heidelberg, Berlin, Heidelberg, 2010.

[8] Léo Milecki, Jonathan Porée, Hatim Belgharbi, Chloé Bourquin, Rafat Damseh, Patrick Delafontaine-Martel, Frédéric Lesage, Maxime Gasse, and Jean Provost. A deep learning framework for spatiotemporal ultrasound localization microscopy. *IEEE Transactions on Medical Imaging*, 40(5):1428–1437, 2021.

[9] Pengfei Song, Joshua D. Trzasko, Armando Manduca, Runqing Huang, Ramanathan Kadirvel, David F. Kallmes, and Shigao Chen. Improved super-resolution ultrasound microvessel imaging with spatiotemporal nonlocal means filtering and bipartite graph-based microbubble tracking. *IEEE Transactions on Ultrasonics, Ferroelectrics, and Frequency Control*, 65(2):149–167, 2018.

[10] Giulia Tuccio, Sajjad Afrakhteh, Giovanni Iacca, and Libertario Demi. Time efficient ultrasound localization microscopy based on a novel radial basis function 2d interpolation. *IEEE Transactions on Medical Imaging*, 2023.

[11] Ruud JG van Sloun, Oren Solomon, Matthew Bruce, Zin Z Khaing, Hessel Wijkstra, Yonina C Eldar, and Massimo Mischi. Super-resolution ultrasound localization microscopy through deep learning. *IEEE transactions on medical imaging*, 40(3):829–839, 2020.